



# AMERICAN METEOROLOGICAL SOCIETY

*Journal of Climate*

## **EARLY ONLINE RELEASE**

This is a preliminary PDF of the author-produced manuscript that has been peer-reviewed and accepted for publication. Since it is being posted so soon after acceptance, it has not yet been copyedited, formatted, or processed by AMS Publications. This preliminary version of the manuscript may be downloaded, distributed, and cited, but please be aware that there will be visual differences and possibly some content differences between this version and the final published version.

The DOI for this manuscript is doi: 10.1175/JCLI-D-14-00284.1

The final published version of this manuscript will replace the preliminary version at the above DOI once it is available.

If you would like to cite this EOR in a separate work, please use the following full citation:

Justino, F., A. Silva, M. Pereira, F. Stordal, D. Lindemann, and F. Kucharsk, 2014: The large-scale climate in response to the retreat of the West Antarctic Ice Sheet. *J. Climate*. doi:10.1175/JCLI-D-14-00284.1, in press.



# The Large-scale Climate in Response to the Retreat of the West Antarctic

## Ice Sheet

F. Justino\* and A. S. Silva†

*Department of Agricultural Engineering , Universidade Federal de Viçosa, Brazil*

M. P. Pereira

*Department of Agricultural Engineering , Universidade Federal de Viçosa, Brazil*

F. Stordal

*Centre for Earth Evolution and Dynamics (CEED),*

*Department of Geosciences, University of Oslo, Norway*

D. Lindemann

*Department of Agricultural Engineering , Universidade Federal de Viçosa, Brazil*

F. Kucharski

*The Abdus Salam International Centre for Theoretical Physics, Trieste, Italy*

\*Corresponding author address: Department of Agricultural Engineering , Universidade Federal de Viçosa, Brazil,

E-mail: [fjustino@ufv.br](mailto:fjustino@ufv.br)

†Department of Agricultural Engineering , Universidade Federal de Viçosa, Brazil

## ABSTRACT

4 Based upon coupled climate simulations driven by present day and condi-  
5 tions resembling the Marine Isotope Stage 31 (WICE-EXP), insofar the West  
6 Antarctic Ice Sheet (WAIS) configuration is concerned, we demonstrate that  
7 changes in the WAIS orography lead to noticeable changes in the oceanic and  
8 atmospheric circulations. Compared with the present day climate, the WICE-  
9 EXP is characterized by warmer conditions in the Southern Hemisphere (SH)  
10 by up to 5°C in the polar oceans and up to 2°C in the Northern Hemisphere  
11 (NH). These changes feed back on the atmospheric circulation weakening  
12 (strengthening) the extratropical westerlies in the SH (northern Atlantic). Cal-  
13 culations of the Southern Annular Mode (SAM) show that modification of the  
14 WAIS induces warmer conditions and a northward shift of the westerly flow,  
15 in particular there is a clear weakening of the polar jet. These changes lead  
16 to modification of the rate of deep water formation reducing the magnitude  
17 of the North Atlantic Deep Water, but enhancing the Antarctic Bottom Water.  
18 By evaluating the density flux we have found that the thermal density flux  
19 has played a main role in the modification of the meridional overturning cir-  
20 culation. Moreover, the climate anomalies between the WICE-EXP and the  
21 present day simulations resemble a bipolar seesaw pattern. These results are  
22 in good agreement with paleoreconstructions in the framework of the Ocean  
23 Drilling and ANDRILL Programs.

## 4 **1. Introduction**

5 The large-scale Earth's topography has long been recognized to influence the climate system  
6 (Justino and Peltier (2006), Hamon et al. (2012), Kageyama and Valdes (2000)). For instance, the  
7 shape of the Antarctic ice sheet can potentially modify the stationary and transient atmospheric  
8 waves, the wind stress and thus the oceanic circulation (e.g. Justino et al. (2014), Knorr and  
9 Lohmann (2014)).

10 Past changes of continental and seaice from 65 to 1 Ma are primarily induced by changes in the  
11 configuration of the astronomical forcing (e.g. Scherer et al. (2008)). Recently, the influence of  
12 the atmospheric CO<sub>2</sub> concentration in leading the onset of the Antarctic glaciation has also been  
13 explored (DeConto and Pollard (2003)). DeConto et al. (2007) argued that once ice sheets are  
14 established, seasonal seaice distribution is highly sensitive to astronomical forcing and ice sheet  
15 geometry due to modification of the regional temperature and low-level winds.

16 As demonstrated by Zachos et al. (2001), the orography of the Antarctic ice sheet has changed  
17 substantially during the history of Earth. Lowering the Antarctic ice sheet height can result in  
18 a thermal forcing associated with the ascending lapse-rate inducing local warming (Justino et al.  
19 (2014)). Moreover, modification of the ice sheet mass balance leads to an anomalous pattern of  
20 the radiative balance due to changes in surface albedo (Pollard and DeConto (2005), Pekar and  
21 DeConto (2006), Pollard et al. (2005)). Of particular interest is the Marine Isotope Stage 31  
22 (MIS31), that occurred  $\sim 1,08$ - $1,07$  Ma (million years ago, see Figure 1) in the early Pleistocene.  
23 This period is characterized by substantial deglaciation of the west Antarctica ice sheet (WAIS,  
24 Naish et al. (2009)). DeConto et al. (2012) using a 3-D ice sheet-shelf and global climate model  
25 to reconstruct the SST and seaice, have demonstrated a nearly complete collapse and subsequent  
26 recovery of marine ice in West Antarctica in the early Pleistocene.

27 These modelling results have been confirmed by The Ocean Driling Program (ODP) sites 1090  
28 and 1165 showing that the MIS31 interval was considerably warmer than present. Additional  
29 support has been given by the marine glacial record of the AND-1B sediment core, recovered from  
30 the Ross ice shelf by the ANDRILL programme. Naish et al. (2009) have in particular documented  
31 astronomically-induced oscillations in the WAIS which collapsed at periodical intervals.

32 Previous investigations of the climate response to Antarctic ice sheet (AIS) variation have  
33 demonstrated that removal of the WAIS may increase the surface temperature by up to 4.9°C  
34 at DOME F and by up to 5.0°C at Dome C (Holden et al. (2010)). Goldner et al. (2013) evaluating  
35 the impact of adding an AIS to a "greenhouse world" mimicking the Eocene, and subtracting the  
36 AIS from the modern Antarctica, argued that the climatic feedbacks induced by the AIS did not  
37 lead to decreasing global mean surface temperature during the Eocene-Oligocene transition.

38 However, the authors demonstrated that the climate response due to the AIS changes is strongly  
39 modulated by the atmospheric CO<sub>2</sub> concentration. The climate response to modifications of the  
40 Antarctic topography has also been studied by Knorr and Lohmann (2014). In evaluating the  
41 role of an AIS expansion in the middle Miocene, it has been found that the ice sheet growth was  
42 accompanied by a warming in the surface waters of the SH Polar Ocean, which has been driven by  
43 atmosphere-ocean feedbacks on the initial wind field. Despite these efforts, the impact of distinct  
44 ice sheet configuration, such as during the MIS31 interval, on the wind driven and the thermohaline  
45 circulation (THC) has not been addressed in details.

46 To investigate the anomalous pattern of the austral seaice and SST DeConto et al. (2007) have  
47 applied the GENESIS climate model coupled to surface model components including a nondy-  
48 namical 50-meter slab ocean. Although this modeling design has improved our understanding of  
49 coupled mechanisms of past climate change, it assumes a fixed deep-to-surface ocean heat flux.  
50 Thus, crucial ocean-atmosphere feedbacks that are important for the reorganization of the large-

51 scale climate are ignored. This limitation, however, can be overcome in coupled modelling  
52 studies using full ocean models. This also allows evaluation of changes in the THC, oceanic and  
53 atmospheric heat fluxes, and it provides a unique opportunity to study the influence of the WAIS  
54 in a global perspective. Moreover, the results can have relevance to both past interglacials when  
55 the WAIS retreated and potentially to future WAIS configurations.

## 56 **2. Coupled climate simulations**

57 In order to investigate the global climate response to retreat of WAIS resembling the WAIS con-  
58 ditions during the MIS31 interval (e.g. seaice, surface temperatures, the THC and oceanic and  
59 atmospheric heat fluxes), two model simulations have been performed with the Speedy-Ocean  
60 (SPEEDO) coupled model (Severijns and Hazeleger (2010)). A modern simulation driven by  
61 present day boundary conditions (MOD) and a second experiment that includes the ice sheet  
62 topography characteristic of the MIS31 interval (WICE-EXP). The MOD experiment has been  
63 described in detail in a previous publication (Justino et al. (2014)). The simulations (MOD and  
64 WICE-EXP) were run to equilibrium for 1000 years and the analyses discussed herein are based  
65 upon the last 50 years of each simulation.

66 The reason for performing a long numerical simulation is because of the need to reach a quasi-  
67 steady state. As stated in Danabasoglu et al. (1996) and according to their approach, the solution  
68 of the present study is defined by a quasi-steady state when the simulated seasonal and annual  
69 cycles become cyclic. This means that the analysed variables show little variation between cycles.  
70 The spin-up time for a given integration remains a topic of debate in the scientific community.  
71 Supposing that the interest is on oceanic equatorial surface fields, this spin-up time can be achieved  
72 with a few years of integration. However for mid-latitudes and deep waters, this time can be much  
73 longer, reaching decadal to centennial time scales.

74 The atmospheric component of the SPEEDO coupled model, called Simplified Parametrization,  
75 primitivE-Equation Dynamics (SPEEDY), is a hydrostatic spectral model with 8 vertical layers  
76 (925, 850, 700, 500, 300, 200, 100 and 30 hPa) and horizontal truncation T30, which corresponds  
77 to a horizontal resolution of  $3.75^\circ$ . It uses the divergence-vorticity equation. The oceanic com-  
78 ponent of the SPEEDO is the Coupled Large-Scale Ice-Ocean model (CLIO, Goosse and Fichefet  
79 (1999)). This model is based on the primitive equations (Navier Stokes equations) and uses free  
80 surface with a thermodynamic/dynamic parameterization of the seaice component. CLIO also  
81 employs a parameterization for vertical diffusivity, which is a simplification of the Mellor and  
82 Yamada turbulence scheme (Mellor and Yamada (1982)).

83 The ability of the SPEEDO model to reproduce basic features of the mean modern climate has  
84 been extensively analysed in Severijns and Hazeleger (2010). For example, the model is able  
85 to reproduce the large-scale mean flow in the Atlantic region and captures the South Atlantic  
86 Convergence Zone. The North Atlantic climatological atmospheric features, such as the mean  
87 and eddy geopotential height and the NAO variability of the atmospheric component of SPEEDO  
88 (SPEEDY), have been shown to compare well with present day observations (Kucharski et al.  
89 (2006)). The atmospheric climatology of SPEEDY is also systematically verified with respect to  
90 observations in [http://users.ictp.it/~kucharsk/speedy8\\_clim\\_v41.html](http://users.ictp.it/~kucharsk/speedy8_clim_v41.html).

91 In order to further evaluate the reliability of SPEEDO to simulate the present day seasonal model  
92 variability, is shown in Figure 2 the first harmonic of precipitation, near air surface temperature  
93 and zonal winds, as well as in the NCEP/NCAR Reanalysis 1 (NNR1) and the Global Precipita-  
94 tion Climatology Project (GPCP). The first order harmonic of meteorological parameters shows  
95 long-term effects, while higher order harmonics show the effects of short-term fluctuations. The  
96 harmonic analysis is a useful tool to characterize different climate regimes and transition regions.

97 Moreover, it provides the possibility to identify dominant climate features in the space-time do-  
98 main.

99 Figures 2a,d show higher seasonality over North America and northeastern Asia with values up  
100 to 30°C, a feature that is properly reproduced by the MOD simulation. Over the SH extratropics,  
101 both datasets agree on an enhanced seasonal cycle over South America, Africa and Australia,  
102 although over oceanic regions the SPEEDO simulation displays weaker seasonality as compared  
103 with the NNR1.

104 Turning to precipitation (Fig. 2b,e), SPEEDO simulates a narrower band of precipitation in the  
105 tropical Atlantic region, thus, smaller amplitude of the seasonal cycle as compared with GPCP. It  
106 should be noted, however, that the MOD simulation reasonably reproduces the annual cycle of pre-  
107 cipitation over the tropical forests of South America, Africa and Indonesia, as well as the precip-  
108 itation pattern associated with monsoonal systems (e.g the Indian and South America monsoons).  
109 Evaluation of the zonal wind seasonal cycle demonstrates that the MOD simulation exhibits higher  
110 amplitude of the northeastern trade winds and the SH extratropical westerly flow compared to the  
111 NNR1. This deficiency around Antarctica may very likely be due to an overestimation of the  
112 winter seaice area which can enhance the seasonal meridional thermal contrast. Elsewhere, the  
113 SPEEDO model can properly reproduce the seasonal fluctuation of the zonal atmospheric flow  
114 evident in the NNR1.

115 Figure 3a shows that in the zonal mean near surface temperature, SPEEDO compares well with  
116 the observed patterns. The largest difference between the model and the observations is located  
117 to the south of 75°S, where the steep topography of Antarctica plays a substantial role. This is  
118 a recurrent limitation in low resolution models as demonstrated by Justino et al. (2010). Sev-  
119 eral known problems have also been identified in the NNR1 in Antarctica as demonstrated by  
120 Chapman and Walsh (2007).



121 Analyses of precipitation (Fig. 3b) demonstrate that the MOD simulation is able to reproduce  
122 the most significant characteristics evident in the NNR1 data. The observed and simulated values  
123 over the equatorial regions associated with the Inter-Tropical Convergence Zone (ITCZ) exceed  
124 6mm/day. The SPEEDO model can also reproduce the NH precipitation pattern in the storm  
125 track regions over the 40°-60°N latitudinal belt. Differences, however, between the simulated and  
126 NNR1 rainfall are found around 40°-60° in the Southern Hemisphere.

### 127 *a. The WICE-EXP Simulation design*

128 The ice sheet reconstruction characteristic of the MIS31 interval has been achieved by applying  
129 a combined ice sheet/ice shelf model, coupled to a high-resolution new treatment of grounding-  
130 line dynamics and ice-shelf buttressing to simulate Antarctic ice sheet variations over the past five  
131 million years (Fig. 1b, Pollard and DeConto (2009)). Figure 1c shows topography anomalies  
132 between these two simulations (WICE-EXP and MOD), that are by up to 2000m located in the  
133 current WAIS region. Elsewhere changes are smaller than 800m.

134 It is important to note that the inclusion of the MIS31 ice sheet topography  
135 (Fig. 1, Pollard and DeConto (2009)) leads to highly significant changes in the shape of the  
136 Antarctica ice sheet, with large ice free areas in west Antarctica. To include the effect of diabatic  
137 heating on the surface radiative balance the surface albedo is modified. In the MOD simulation  
138 the Antarctic ice sheet albedo is  $\sim 70\%$ , an intermediate value between the bare ice (54%) and  
139 snowfall (85%). In the WICE-EXP the albedo over ice free regions is computed by the oceanic  
140 model component. It should be noted that present time estimates of albedo based on observations  
141 in Antarctica are restricted to a few locations. Nevertheless, model estimates have proposed an ice  
142 sheet albedo varying from 70 to 85% (Munneke et al. (2011)).

143 Both simulations are run under atmospheric CO<sub>2</sub> concentration of 380 ppm and present day  
144 astronomical configuration. This allows for an isolated evaluation of the climatic effect associ-  
145 ated with the WAIS collapse. It is important to notice that the MIS31 event experiment does not  
146 cover all aspects of this period. However, the sensitivity experiment can be applied to any "super-  
147 interglacial" of the early Pleistocene, or any of the periods in the Pliocene with a collapsed WAIS,  
148 when it comes to an investigation of changes in topography and albedo of the AIS.

#### 149 *b. Atmospheric circulation*

150 The annual mean near surface air temperature (T<sub>2m</sub>) under present day conditions (Fig. 4a) ex-  
151 hibits the characteristic pattern with milder (warmer) temperatures over the extratropics (tropics),  
152 and lower temperature in the polar regions over Antarctica due to high continental elevation and  
153 the seaice effect. Turning to changes between the two simulations (MOD and WICE-EXP, Fig.  
154 4b), it is evident that warming has occurred under WICE-EXP as compared with modern condi-  
155 tions. Furthermore, the SH warming also extends significantly northward over the tropical region  
156 and mid-latitudes, in particular over the western hemisphere. It should be noted that most changes  
157 in T<sub>2m</sub> are statistically significant at 95% level based on the t-test. Temperature differences over  
158 the western Antarctica, where changes in topography are largest, can reach values as high as 7°C  
159 (Fig. 4b). Over the eastern part of Antarctica lower temperatures are noted in the WICE-EXP  
160 by up to -5°C, compared to the MOD run. The simulated WICE-EXP warming/cooling over the  
161 ice cap is due to the combined direct and indirect influences of lapse-rate effect which follows  
162 changes in topography, in particular the collapse of the WAIS. This is opposite to what has oc-  
163 curred during the Last Glacial Maximum (LGM), in the sense that during the LGM the WAIS  
164 was approximately 1000m higher than presently (e.g Whitehouse et al. (2012), Justino and Peltier  
165 (2006), Peltier (2004)). Interior ice elevations of the WAIS remains, however, uncertain. Ackert

166 et al. (2007) propose a WAIS approximately 125 m above the present surface during the 11.5 ka  
167 interval.

168 Over the polar oceans, anomalies are associated with enhanced warm advection from reduced  
169 WAIS and increased oceanic heat flux due to the substantial reductions in seaice thickness. It  
170 is important to note that the reduction in seaice area induces the albedo-seaice-ocean feedback  
171 leading to further warming. Over the mid-latitudes and tropics the WICE-EXP warming may be  
172 primarily related to weaker surface winds, and reduced evaporative cooling. It should be noted  
173 that colder conditions over the northern Atlantic are found in the region of deep water formation.  
174 This is in line with enhanced surface winds, as will be discussed later.

175 A brief comparison between the WICE-EXP results and the Pliocene Model Intercomparison  
176 Project (PlioMIP, Haywood et al. (2010)) demonstrates many similarities. For instance, Chan et al.  
177 (2011) and Haywood et al. (2009), based on OAGCM simulations, report higher zonal averaged  
178 air temperature at high latitudes by up to 5°C accompanied by a decrease in the equator-to-pole  
179 temperature gradient (Zhang et al. (2012)). A large increase can be found in particular at polar  
180 latitudes. Indeed, this warming is a common feature in the PlioMIP: experimental design, mid-  
181 Pliocene boundary conditions and implementation special issue  
182 ([http://www.geosci-model-dev.net/special\\_issue5.html](http://www.geosci-model-dev.net/special_issue5.html)).

183 In WICE-EXP the anomalous pattern of temperatures modifies the meridional thermal gradi-  
184 ent and therefore the surface wind configuration. These changes in the thermal structure of the  
185 atmosphere are in accordance with the thermal wind relation which suggests a weakening of the  
186 westerly flow in the WICE-EXP simulation. The wind magnitude (Fig. 4d) reveals a substantial  
187 slowdown of the polar jet and the extratropical westerlies, however the sub-tropical jet has been  
188 strengthened around 30°S. This is particularly evident over the subtropical Atlantic ocean.

189 Turning to the Northern Hemisphere (NH), one may note an enhancement of the trade winds  
190 and the mid-latitude westerly flow which is clearly depicted over the Atlantic and Pacific basins.  
191 Hence, warmer air advection is expected to be intensified over Scandinavia and Eurasia leading to  
192 warmer temperatures in the WICE-EXP as compared with the MOD simulation (Fig. 4b).

193 Changes in temperature and surface winds are also associated with modification in the geopotential  
194 height at 700hPa (GH700, Fig. 4e,f). The main observed features of the present day stationary  
195 waves in the SH are reasonably reproduced in our MOD simulation. Despite the coarse spatial  
196 resolution of the SPEEDO atmospheric component, the model is able to reproduce the current low  
197 pressure system over the Ross and Amundsen-Bellingshausen seas (Hosking et al. (2013)).

198 The absence of the WAIS leads to highly significant changes in GH700 (Fig. 4f), in particular  
199 over the mainland of Antarctica and oceanic regions south of 50°S. This is primarily due to  
200 increased thickness of the column caused by enhanced lower tropospheric warming (Fig. 4b,f).  
201 Further analysis demonstrates that over the subtropical Atlantic ocean near the South America  
202 coast and around the 40°S latitudinal belt over Australia and the Pacific ocean, GH700 contracts  
203 so as to become of lesser extent as compared with modern conditions.

204 One should keep in mind that the substantial warming over west Antarctic in the WICE-EXP  
205 leads to distinct SH climate symmetry, which modified the spatial-temporal polar climate variability  
206 associated with the SAM, as will be discussed later. Justino and Peltier (2005) argued that the  
207 polar climate variability is strongly modulated by the direct mechanical effect of ice sheet topog-  
208 raphy (lapse rate), and by the effect of diabatic heating due to the marked change in the spatial  
209 variation of surface albedo.

210 The Z700 changes in the NH show an intensification of the Azores high and a deepening of  
211 the Icelandic low (Fig. 4f). This feature may indicate an intensification of the positive phase  
212 of the North Atlantic Oscillation (NAO). During the positive phase of the NAO, warmer condi-

213 tions are observed in Scandinavia that are accompanied by increased maritime air advection and  
214 strong westerly flow over the northern Atlantic. These patterns are well reproduced by the climate  
215 anomalies between the WICE-EXP and the MOD simulations.

216 The precipitation pattern depicted in the SH subtropics by the MOD simulation is primarily  
217 dominated in the Pacific and Indian Oceans by the influence of the recurrent baroclinic systems  
218 (Fig. 4g). In South America the precipitation band is primarily associated with the South Atlantic  
219 Convergence Zone (Fig. 4g). Also evident is the precipitation in the storm track region of the  
220 north Atlantic and Pacific.

221 In comparison with the MOD simulation, the WICE-EXP shows a decrease in precipitation in  
222 the tropical oceans, except over the Pacific (Fig. 4h). Positive anomalies are noted in the subtropics  
223 in the SH which are statistically significant. It is interesting to stress that the subtropical region  
224 experiences a substantial increase in precipitation related to the northward displacement of the main  
225 baroclinic zone due to changes in the meridional thermal gradient. These areas are also placed in  
226 good agreement with areas with reduced GH700 (Fig. 4f). Changes in the NH are weaker, although  
227 increased precipitation is evident in the northern Atlantic storm track region and in eastern Asia/  
228 Pacific.

### 229 *c. Southern Annular Mode*

230 Based upon comparison of the MOD and WICE-EXP climates, in what follows the impact of  
231 these differences upon the spatial structure of the Southern Annular Mode (SAM) and its related  
232 features are investigated. SAM is responsible for the migration of the subtropical upper-level jet  
233 and variations in the intensity of the polar jet (Carvalho et al. (2005)), as well as for the intensi-  
234 fication of an upper-level anticyclonic anomaly, weakened moisture convergence, and decreased  
235 precipitation over southeastern South America. Empirical orthogonal function (EOF) analysis has

236 been performed on Z700 monthly data throughout the 50 years of each model experiment. SAM  
237 is displayed in terms of the spatial pattern of its amplitude (Fig. 5), obtained by regressing the  
238 hemispheric Z700 anomalies upon the monthly leading principal component (PC) time series.

239 The leading pattern of variability in the MOD simulation (Fig. 5a) is characterized by an annu-  
240 lar structure over the entire hemisphere which is dominated by two areas of strong out-of-phase  
241 variability located over mid-latitudes ( $40^{\circ}$ - $55^{\circ}$ S) and the polar region (Fig. 5a). Although differ-  
242 ences may be identified between our modeled SAM and the SAM resulting from climate system  
243 models of higher complexity (e.g Justino and Peltier (2006), L'Heureux and Thompson (2006)),  
244 it is evident that the SPEEDO provides a reasonable depiction of this atmospheric mode, charac-  
245 teristic wave number 3 . The first modeled EOF accounts for 54% of the total variance and is well  
246 separated from the second EOF which explains 6%. The temperature response to SAM is shown  
247 in Figure 5b. Fluctuations of SAM lead, during the positive phase, to slightly warmer near surface  
248 (colder) conditions in the subtropical (polar) region. This warming is evident in the southern At-  
249 lantic and southern South America regions and over the Antarctic peninsula, over Australia and  
250 the Tasman Sea, and southern Africa. It should be emphasized that during the positive phase of  
251 SAM our MOD simulation predominantly indicates positive near surface temperature anomalies  
252 globally (Fig. 5b). These characteristics are accompanied by weaker (stronger) westerlies in the  
253 vicinity of  $30^{\circ}$ S -  $45^{\circ}$ S ( $45^{\circ}$  -  $60^{\circ}$ S, Fig. 5c).

254 Figure 5d shows the differences between SAM (first EOF of Z700) as a result of modification  
255 in the WAIS structure along with the modeled present day SAM. It should be noted that SAM  
256 in the WICE-EXP is no longer characterized by a predominant dipolar structure and it explains  
257 48% of the climate variability, i.e lower variance as compared with the present day SAM. For  
258 instance, meridional changes in Z700 between the polar and extratropical regions in the MOD  
259 simulation may reach values up to 70 hPa, whereas in the WICE-EXP values do not exceed 30

260 hPa. Moreover, the well defined high pressures centres under MOD conditions are much weaker  
261 in the WAIS collapsed situation (Fig. 5d).

262 However, the southern Atlantic anticyclone is intensified which may increase the oceanic mois-  
263 ture advection to the subtropical part of South America (Fig. 5d). It should be noted, moreover,  
264 that the strengthening of this mid-latitude center of action in the WICE-EXP reduces the migra-  
265 tion of colder extratropical air masses, creating a blocking situation. This further reduces the sea-  
266 sonal climate variability in South America/southern Atlantic. The opposite is found over southern  
267 Africa/Indian ocean and subtropical Pacific (Fig. 5d). Carvalho et al. (2005) discussed the de-  
268 gree of involvement of the seasonal subtropical climate and SAM, and the existence of strong  
269 teleconnection between the polar and subtropical regions in the SH has been demonstrated.

270 SAM-induced modification of the near surface temperature by changes in the WAIS (Fig. 5e)  
271 shows strong warming over the Antarctica peninsula/Bellinghausen sea as well as over the polar  
272 ocean between 0-150°E. Over the eastern hemisphere, this clearly reflects the weakening of the  
273 SAM in the WICE-EXP. However, over the western hemisphere including the Antarctica penin-  
274 sula, this cannot be assumed because SAM is no longer characterized by the annular structure.  
275 In terms of changes in the zonal wind, we found negative (positive) anomalies in the polar re-  
276 gion (subtropics) and intensified wind curl in the WICE-EXP, as compared with the present day  
277 simulation (Fig. 5f).

278 These climate anomalies between the MOD and the WICE-EXP experiments and the differences  
279 between the climate response to SAM in the two simulations, reveal that despite the small area of  
280 the WAIS compared with the entire Antarctica, it plays a prominent role in setting up the SH  
281 atmospheric conditions.

282 *d. Oceanic conditions*

283 In what follows is discussed the role of the WAIS topography upon the oceanic conditions.  
284 Despite the low resolution of our oceanic component, the coupled model is able to simulate the  
285 intensified SST meridional thermal contrast (cold tongue) along the western coastal margins of  
286 South America as well as the coastal upwelling in Africa (Fig. 6a). It should be noted that a  
287 thorough evaluation of the present climate has been provided by Justino et al. (2014) and Severijns  
288 and Hazeleger (2010). As should be expected, changes in SST exhibit many similarities with the  
289 near surface air temperature anomalies (Figs. 4b, 6a), in particular in the extratropical region.

290 It is interesting to note that compared with the MOD simulation, WICE-EXP shows warmer  
291 conditions primarily confined in the SH. However, the warming along the latitudinal belt between  
292 30-60°S shows values as high as 4°C in the southern Atlantic. Lower SSTs up to -2°C are found in  
293 the northern Pacific and Atlantic. This SST anomalous pattern resembles the oceanic response to  
294 increased freshwater into the northern Atlantic during the last glacial cycle (e.g. Rahmstorf (1996),  
295 Manabe and Stouffer (1995), Knutti et al. (2004)). These investigations suggested that changes  
296 in the rate of deep water formation and subsequently the reduction in the meridional oceanic heat  
297 transport was the primary contributor to the existence of the bipolar seesaw (Broecker (1998)).  
298 This assumption is further analysed in our study.

299 Figure 6c shows the present day seaice as simulated by the MOD run. Sea ice has a direct im-  
300 pact on the radiation budget of the climate system by affecting the net incoming solar radiation  
301 due to its high albedo (i.e. decreasing the absorption of solar radiation). Therefore, modification  
302 of the seaice cover may induce warming/cooling due to the seaice albedo feedback. As com-  
303 pared with satellite data, Severijns and Hazeleger (2010) argued that the seaice representation in



304 SPEEDO yields understimation of seaice in late summer and overstimation in late winter in both  
305 hemispheres.

306 Present day seaice thickness can reach values in the SH by up to 1m in the Weddell Sea and  
307 up to 1.2m in the Arctic ocean (Fig. 6c). Figure 6d shows that changes in the WAIS lead to  
308 substantial reduction in the seaice thickness in both hemispheres. This is more evident in the  
309 Weddell and Bellingshausen seas, where atmospheric induced SST anomalies are the primary  
310 candidate to impose these changes. The importance of the wind field for leading changes in seaice  
311 has been explored by Lefebvre et al. (2004).

312 Figures 6e and 6f show the vertical distribution of zonally averaged ocean temperature anoma-  
313 lies, globally (Fig. 6e) and for the Atlantic basin (Fig. 6f). Globally the ocean temperature shows  
314 an overall warming from 60°S to 50°N in the WICE-EXP in comparison with the MOD simu-  
315 lation, which is more pronounced in the Southern Hemisphere down to 1000m depth. However,  
316 underneath this level lower temperatures are simulated in the WICE-EXP as compared with the  
317 MOD run.

318 In the Atlantic sector there has been an oceanic warming down to 1500m with values as high  
319 as 4.5°C. Below 1500m the ocean temperatures are much lower than the global average in the  
320 Atlantic. Marshall and Speer (2012) also argue that warmer surface conditions in the vicinity  
321 of the Antarctic continent may be related to water supplied from deeper layers along inclined  
322 outcropping density surfaces.

323 This vertical distribution of temperature may modify deep convection in the main sites of deep  
324 water formation. Indeed, this has been found to be the case. Figure 7 shows the anomalous pattern  
325 of the Meridional Overturning Circulation (MOC) as delivered by the WICE-EXP simulation.  
326 These results have demonstrated that the absence of the WAIS produces a remarkable weakening  
327 in the southward flow of the MOC (i.e North Atlantic Deep Water, NADW), as compared with

328 present day conditions. It is also evident (Fig. 7 top) that the northward returning flow (e.g.  
 329 Antarctic Bottom Water, AABW) is intensified in the interior ocean. One may argue that this  
 330 oceanic feature may be related to increased loss of heat to the atmosphere in the SH polar ocean  
 331 and therefore enhanced downwelling.

332 It should be stressed that an additional contribution to this anomalous MOC in the WICE-EXP  
 333 simulation, in particular in the SH, may arise from an anomalous Deacon cell which is primarily  
 334 linked to the westward atmospheric flow (Marshall and Speer (2012), Speer et al. (2000)) .

335 To further investigate these changes we have computed the annual density flux as proposed by  
 336 Schmitt et al. (1989) and Speer and Tziperman (1992). The surface density anomalies (a combina-  
 337 tion of the thermal and the haline density anomalies) have the potential to generate thermohaline  
 338 circulation changes. To evaluate the thermal and haline contributions to the density changes in  
 339 WICE-EXP, the thermal and haline components of the density flux ( $kgm^{-2}s^{-1}$ , Fig. 7a,b) are  
 340 computed. The surface density flux based on Schmitt et al. (1989),

341

$$F_{\rho} = \alpha F_t + \beta F_S = -\alpha \frac{Q}{C_P} + \beta \rho \frac{(E - P - R - I)S}{1 - S}, \quad (1)$$

342 includes the thermal expansion ( $\alpha = -\frac{1}{\rho} \frac{\partial \rho}{\partial T} |_{p,S}$ ) and the haline contraction coefficient ( $\beta =$   
 343  $\frac{1}{\rho} \frac{\partial \rho}{\partial S} |_{p,T}$ ). In these expressions,  $C_P, \rho, p, T$  and  $S$  are specific heat, density, pressure, sea  
 344 surface temperature and salinity, respectively.  $Q, E, P, R$  and  $I$  represent net heat flux, evaporation,  
 345 precipitation, runoff and water flux by sea-ice melting and growth, respectively.

346 In the northern Hemisphere (not shown) there are two regions of strong density gain; in the  
 347 western North Atlantic, where cold and dry continental air masses blow onto relatively warm  
 348 waters of the Gulf Stream and North Atlantic Current. The second region of density gain is in  
 349 the Nordic Seas, due to a negative net heat flux associated to strong cooling of surface waters.

350 The contribution of the haline density flux to the total density is much smaller. However, it may  
351 dominate the density gain at the ice/water interface.

352 Figure 7 shows the surface density flux for MOD and the anomalies between WICE-EXP and  
353 MOD. Under present day conditions the region of strongest density gain is located in the Antarctic  
354 continental margins, in particular in the Ross and Bellingshausen Seas (Fig. 7a,b). This is pri-  
355 marily associated with the dominance of cold air embedded in the westerly flow and due to the  
356 influence of katabatic winds. The second region of density gain is the southern Atlantic, where the  
357 model experiences a negative net heat flux associated with strong cooling of surface waters. The  
358 areas of density loss around the 30°-60°S correspond to areas where precipitation/snowfall excess  
359 linked to the storm track dynamics is expected (Fig. 7b,c).

360 As for present-day climate, the simulated deep water formation in WICE-EXP is also controlled  
361 by the thermal density flux. Due to the stronger vertical gradient of temperature in the ocean-  
362 atmosphere interface, the thermal density flux anomalies (Fig. 7d) generate substantial changes  
363 in the surface density (not shown). An increase in the vertical air-sea temperature contrast, and  
364 therefore the loss of heat from the ocean to the atmosphere, leads to strong convective mixing and  
365 an enhancement of the SH deep water formation in WICE-EXP.

366 The total (thermal+haline) density flux anomalies are dominated by changes in the thermal flux.  
367 Haline flux anomalies are most important over the 30°-60°S latitudinal belt. These findings serve  
368 to highlight the importance of the WAIS for the rate of formation of the SH branch of the MOC,  
369 in particular for the formation of the deep water in the Ross/Bellingshausen sea and the southern  
370 Atlantic.

371 Paleoreconstructions focusing on the MIS31 period (e.g. Streng et al. (2011), Scherer et al.  
372 (2008)) have shown periodic seaice-free conditions at the time, in particular in the Ross Sea. As  
373 demonstrated by Scherer et al. (2008) sea surface temperatures were 3-5°C warmer than present

374 day. Evaluations of deep-sea sediments recovered at ODP sites 1094 and 1165 (Maiorano et al.  
375 (2009), Flores and Sierro (2007)) revealed that the absence of the WAIS leads to a southward  
376 displacement of the polar front in the South Atlantic sector. These anomalous patterns indicated  
377 by the reconstruction are reasonably simulated by our climate model experiments presented here.  
378 It should be stressed that the similarities between the modelling results and reconstructions dis-  
379 cussed above solely consider the spatial pattern of differences between the MOD and WICE-EXP  
380 simulations due to the limitation of the modelling setup in terms of boundary conditions. Thus,  
381 our work is not intended to provide a truly realistic account of the reconstructions.

### 382 **3. Summary and concluding remarks**

383 Through two 1000 years coupled climate simulations of present day and a sensitivity experi-  
384 ment taking into account the reduced WAIS topography, we have demonstrated that changes of  
385 the West Antarctic Ice Sheet (WAIS) orography leads to remarkable changes in the oceanic and  
386 atmospheric circulations. In the WICE-EXP simulation, the Southern Hemisphere warms by up  
387 to 8°C in the polar oceans whereas the Northern Hemisphere warms by up to 2°C in comparison  
388 with the present day climate. Hence, seaice is reduced in the both hemispheres SH. These changes  
389 induce a weakening (strengthening) of the extratropical westerlies in the SH (northern Atlantic) in  
390 agreement with the thermal wind relation.

391 Changes in the WAIS also induce an anomalous pattern of temperature and westerlies associ-  
392 ated with SAM. Indeed, a northward shift of the westerly flow and a weakening of the polar jet  
393 have been identified. These changes lead to modification in the rate of deep water formation re-  
394 ducing the magnitude of the North Atlantic Deep Water but enhancing the Antarctic Bottom Water  
395 formation. By evaluating the density flux we argue that the thermal density flux plays the main role  
396 for the modification of the meridional overturning circulation. Moreover, the climate anomalies

397 between the WICE-EXP and the MOD simulations resemble the bipolar seesaw pattern (Broecker  
398 (1998)).

399 One may assume that the magnitude of the idealized ocean's response to fresh water input (as  
400 WAIS retreated), compared with the response to mechanical/topographic atmospheric forcing,  
401 should be weaker, particularly for changes in the deep water formation. Stouffer et al. (2007)  
402 argued that due to the climatological surface winds, which induce surface water northward, fresher  
403 sea surface water in the Southern Ocean will be spread into the other ocean basins.

404 Studies such as Aiken (2008), investigating the role of sea ice in the global climate system,  
405 demonstrated that a fresh water forcing equivalent to 100-yr melt of Southern Hemisphere sea ice  
406 leads to surface cooling but subsurface warming related to decreased overtuning. It is claimed,  
407 however, that those responses are weak, and the initial state recovers over decades. Additional 0.4  
408 Sv of freshwater to the seaice melting experiment also confirms the relatively weak response of  
409 the SH to such forcing.

410 By using a three-dimensional Earth system model of intermediate complexity (EMIC), Swinge-  
411 douw et al. (2008) argued that the climatic impact of AIS melting is primarily induced by interac-  
412 tions with the ocean and sea ice, and less dependent on fresh water discharge.

413 The lack of integrated paleoclimate data as well as the absence of astronomical and CO<sub>2</sub> forcing  
414 in our experiment, limit the value of a detailed data-model comparison with the MIS31 epoch.  
415 The MIS31 interglacial occurred during an extreme peak in astronomical eccentricity that pro-  
416 duced very high austral summer insolation anomalies, followed by very intense boreal summers  
417 approximately 10,500 yrs later. If accounted for here, this certainly would have impacted the  
418 model results. However, generic sensitivity test of the global response to a smaller WAIS, as pre-  
419 sented here, have relevance to both past interglacials when WAIS retreated and possibly to the  
420 future when the WAIS can be affected by the anthropogenic forcing.

421 *Acknowledgments.* We are pleased to acknowledge useful conversations with David Pollard on  
422 the subject of this paper and for making available the topography files. The authors would like  
423 to thank three anonymous reviewers for their valuable contributions. Research support has been  
424 provided through the FAPEMIG grant 551-13 and CNPq 407681.

## 425 **References**

426 Ackert, R. P., S. Mukhopadhyay, B. R. Parizek, and H. W. Borns, 2007: Ice elevation near the  
427 west antarctic ice sheet divide during the last glaciation. *Geophysical Research Letters*, **34** (21),  
428 n/a–n/a, doi:10.1029/2007GL031412, URL <http://dx.doi.org/10.1029/2007GL031412>.

429 Aiken, C. M. M. H. E., 2008: Sensitivity of the present-day climate to freshwater forcing associ-  
430 ated with antarctic sea ice loss. *Journal of Climate*, **21**, 3936–3946, doi:10.1175/2007JCLI1901.  
431 1.

432 Broecker, W., 1998: Paleocean circulation during the last deglaciation. A bipolar seesaw? *Paleo-*  
433 *ceanography*, **13**, 119–121.

434 Carvalho, L. M. V., C. Jones, and T. Ambrizzi, 2005: Opposite phases of the Antarctic Oscillation  
435 and Relationships with Intraseasonal to Interannual activity in the tropics during the Austral  
436 Summer. *J.Clim.*, (18), 702–718.

437 Chan, W.-L., A. Abe-Ouchi, and R. Ohgaito, 2011: Simulating the mid-pleistocene climate with  
438 the miroc general circulation model: experimental design and initial results. *Geoscientific*  
439 *Model Development*, **4** (4), 1035–1049, doi:10.5194/gmd-4-1035-2011, URL [http://www.  
440 geosci-model-dev.net/4/1035/2011/](http://www.geosci-model-dev.net/4/1035/2011/).

441 Chapman, W., and J. Walsh, 2007: A synthesis of Antarctic temperatures. *J. Clim.*, **20**, 4096–4117.

- 442 Danabasoglu, G., J. C. McWilliams, and W. G. Large, 1996: Approach to equilib-  
443 rium in accelerated global oceanic models. *Journal of Climate*, **9** (5), 1092–1110,  
444 doi:10.1175/1520-0442(1996)009<1092:ATEIAG>2.0.CO;2, URL [http://dx.doi.org/10.1175/  
445 1520-0442\(1996\)009<1092:ATEIAG>2.0.CO;2](http://dx.doi.org/10.1175/1520-0442(1996)009<1092:ATEIAG>2.0.CO;2).
- 446 DeConto, R., D. Pollard, and D. Harwood, 2007: Sea ice feedback and Cenozoic evolution of  
447 Antarctic climate and ice sheets. *Paleocenography*, **22**, doi:10.1029/2006PA001350.
- 448 DeConto, R. M., and D. Pollard, 2003: Rapid Cenozoic glaciation of Antarctica induced by de-  
449 clining atmospheric CO<sub>2</sub>. *Nature*, doi:10.1038/nature01290.
- 450 DeConto, R. M., D. Pollard, and D. Kowalewski, 2012: Modeling antarctic ice sheet and cli-  
451 mate variations during marine isotope stage 31. *Global and Planetary Change*, **8889** (0), 45 –  
452 52, doi:<http://dx.doi.org/10.1016/j.gloplacha.2012.03.003>, URL [http://www.sciencedirect.com/  
453 science/article/pii/S0921818112000434](http://www.sciencedirect.com/science/article/pii/S0921818112000434).
- 454 Flores, J.-A., and F. J. Sierro, 2007: Pronounced mid-pleistocene southward shift of the polar  
455 front in the atlantic sector of the southern ocean. *Deep Sea Research Part II: Topical Stud-  
456 ies in Oceanography*, **54** (21), 2432 – 2442, doi:<http://dx.doi.org/10.1016/j.dsr2.2007.07.026>,  
457 URL <http://www.sciencedirect.com/science/article/pii/S0967064507001816>, paleoceanography  
458 and Paleoclimatology of the Southern Ocean A Synthesis of Three Decades of Scientific Ocean  
459 Drilling.
- 460 Goldner, A., M. Huber, and R. Caballero, 2013: Does antarctic glaciation cool the world? *Climate  
461 of the Past*, **9** (1), 173–189, doi:10.5194/cp-9-173-2013, URL [http://www.clim-past.net/9/173/  
462 2013/](http://www.clim-past.net/9/173/2013/).

- 463 Goosse, H., and T. Fichefet, 1999: Importance of ice-ocean interactions for the global ocean  
464 circulation: a model study. *J. Geophys. Res.*, **104(C10)**, 23 337–23 355.
- 465 Hamon, N., P. Sepulchre, Y. Donnadieu, A.-J. Henrot, L. Franois, J.-J. Jaeger, and G. Ramstein,  
466 2012: Growth of subtropical forests in miocene europe: The roles of carbon dioxide and antarctic  
467 ice volume. *Geology*, **40 (6)**, 567–570, doi:10.1130/G32990.1, URL <http://geology.gsapubs.org/content/40/6/567.abstract>, <http://geology.gsapubs.org/content/40/6/567.full.pdf+html>.
- 469 Haywood, A. M., M. A. Chandler, P. J. Valdes, U. Salzmann, D. J. Lunt, and H. J. Dowsett, 2009:  
470 Comparison of mid-pliocene climate predictions produced by the hadam3 and {GCMAM3}  
471 general circulation models. *Global and Planetary Change*, **66 (34)**, 208 – 224, doi:<http://dx.doi.org/10.1016/j.gloplacha.2008.12.014>, URL <http://www.sciencedirect.com/science/article/pii/S0921818108002142>.
- 474 Haywood, A. M., and Coauthors, 2010: Pliocene model intercomparison project (pliomip): experi-  
475 mental design and boundary conditions (experiment 1). *Geoscientific Model Development*, **3 (1)**,  
476 227–242, doi:10.5194/gmd-3-227-2010, URL <http://www.geosci-model-dev.net/3/227/2010/>.
- 477 Holden, P. B., N. R. Edwards, E. W. Wolff, N. J. Lang, J. S. Singarayer, P. J. Valdes, and  
478 T. F. Stocker, 2010: Interhemispheric coupling, the west antarctic ice sheet and warm antarctic  
479 interglacials. *Climate of the Past*, **6 (4)**, 431–443, doi:10.5194/cp-6-431-2010, URL <http://www.clim-past.net/6/431/2010/>.
- 481 Hosking, J. S., A. Orr, M. J. Gareth, J. Turner, and T. Philips, 2013: Energy and numerical weather  
482 prediction. *J. Climate*, **26**, 6633–6648, doi:10.1175/JCLIM-D-12-00813.1.
- 483 Justino, F., J. Marengo, F. Kucharski, F. Stordal, J. Machado, and M. Rodrigues, 2014: Influe-  
484 nce of antarctic ice sheet lowering on the southern hemisphere climate: modeling experiments



485 mimicking the mid-miocene. *Climate Dynamics*, 1–16, doi:10.1007/s00382-013-1689-9, URL  
486 <http://dx.doi.org/10.1007/s00382-013-1689-9>.

487 Justino, F., and W. Peltier, 2006: Influence of Present Day and Glacial Surface  
488 Conditions on the Antarctic Oscillation/Southern Annular Mode. *Geophys. Res. Lett.*,  
489 doi:10.1029/2006GL027001.

490 Justino, F., and W. R. Peltier, 2005: The glacial North Atlantic Oscillation. *Geophys. Res. Lett.*,  
491 **32**, L21 803, doi:10.1029/2005GL023822.

492 Justino, F., A. Setzer, T. J. Bracegirdle, D. Mendes, A. Grimm, G. Dechiche, and C. E. G. R. Schae-  
493 fer, 2010: Harmonic analysis of climatological temperature over Antarctica: present day and  
494 greenhouse warming perspectives. *Internation Journal of Climatology*, doi: 10.1002/joc.2090.

495 Kageyama, M., and P. Valdes, 2000: Impact of the north american ice-sheet orography on the last  
496 glacial maximum eddies and snowfall. *Geophys. Res. Lett.*, **27 (10)**, 1515–1518.

497 Knorr, G., and G. Lohmann, 2014: Climate warming during antarctic ice sheet expansion at the  
498 middle miocene transition. *Nature Geoscience*, **7**, 376–381, doi:10.1038/ngeo2119.

499 Knutti, R., J. Flueckiger, T. Stocker, and A. Timmermann, 2004: Strong hemispheric coupling  
500 of glacial climate through continental freshwater discharge and ocean circulation. *Nature*, **430**,  
501 851–856.

502 Kucharski, F., F. Molteni, and A. Bracco, 2006: Decadal interactions between the western tropical  
503 Pacific and the North Atlantic Oscillation. *Clim. Dyn.*, **26**, 79–91.

504 Lefebvre, W., H. Goosse, R. Timmermann, and T. Fichefet, 2004: Influence of the Southern An-  
505 nular Mode on the sea ice-ocean system. *J. Geophys. Res.*, **109**, doi:10.1029/2004JC002403.

- 506 L'Heureux, M. L., and D. W. J. Thompson, 2006: Observed Relationships between the El Niño  
507 Southern Oscillation and the Extratropical Zonal-Mean Circulation. *J. Clim.*, **19** (2), 276–287.
- 508 Maiorano, P., M. Marino, and J.-A. Flores, 2009: The warm interglacial marine isotope stage 31:  
509 Evidences from the calcareous nannofossil assemblages at site 1090 (southern ocean). *Marine*  
510 *Micropaleontology*, **71** (34), 166 – 175, doi:<http://dx.doi.org/10.1016/j.marmicro.2009.03.002>,  
511 URL <http://www.sciencedirect.com/science/article/pii/S0377839809000255>.
- 512 Manabe, S., and R. J. Stouffer, 1995: Simulation of abrupt climate change induced by freshwater  
513 input to the North Atlantic Ocean. *Nature*, **378**, 165–167.
- 514 Marshall, J., and K. Speer, 2012: Closure of the meridional overturning circulation through south-  
515 ern ocean upwelling. *Nature Geoscience*, **5**, 1710–180.
- 516 Mellor, G., and T. Yamada, 1982: Development of a turbulence closure model for geophysical  
517 fluid problems. *Rev. Geophys. Space Phys.*, **20**, 851–875.
- 518 Munneke, P., Kuipers, M. R. van den Broeke, J. T. M. Lenaerts, M. G. Flanner, A. S. Gardner,  
519 and W. J. van de Berg, 2011: A new albedo parameterization for use in climate models over  
520 the antarctic ice sheet. *Journal of Geophysical Research: Atmospheres*, **116** (D5), n/a–n/a, doi:  
521 [10.1029/2010JD015113](http://dx.doi.org/10.1029/2010JD015113), URL <http://dx.doi.org/10.1029/2010JD015113>.
- 522 Naish, T., and Coauthors, 2009: Obliquity-paced pliocene west antarctic ice sheet oscilla-  
523 tions. *Nature*, **458** (7236), 322–328, URL <http://www.scopus.com/inward/record.url?eid=2-s2.0-62649146401&partnerID=40&md5=4e09abf599f8dff4361f5ce5927d7648>, cited By (since  
524 1996)177.  
525
- 526 Pekar, S. F., and R. M. DeConto, 2006: High-resolution ice-volume estimates for the early  
527 miocene: Evidence for a dynamic ice sheet in antarctica. *Palaeogeography, Palaeoclimatol-*

528 *ogy, Palaeoecology*, **231** (12), 101–109, doi:10.1016/j.palaeo.2005.07.027, URL <http://www.sciencedirect.com/science/article/pii/S0031018205004839>.

530 Peltier, W., 2004: Global glacial isostasy and the surface of the ice-age Earth: the ICE-5G (VM2) model and GRACE. *Annual Review of Earth and Planetary Sciences.*, **32**, 111–149.

532 Pollard, D., and R. DeConto, 2009: Modelling west antarctic ice sheet growth and collapse through the past five million years. *Nature*, <http://dx.doi.org/10.1038/nature07809>.

534 Pollard, D., and R. M. DeConto, 2005: Hysteresis in cenozoic antarctic ice-sheet variations. *Global and Planetary Change*, **45**, 9 – 21, doi:10.1016/j.gloplacha.2004.09.011, URL <http://www.sciencedirect.com/science/article/pii/S0921818104001377>, *ice:title* Long-term changes in Southern high-latitude ice sheets and climate, the Cenozoic history *ice:title*.

538 Pollard, D., R. M. DeConto, and A. A. Nyblade, 2005: Sensitivity of cenozoic antarctic ice sheet variations to geothermal heat flux. *Global and Planetary Change*, **49**, 63 – 74, doi:10.1016/j.gloplacha.2005.05.003, URL <http://www.sciencedirect.com/science/article/pii/S0921818105001049>.

542 Rahmstorf, S., 1996: On the freshwater forcing and transport of the atlantic thermohaline circulation. *Climate Dynamics*, **4**, 73–79.

544 Scherer, R. P., and Coauthors, 2008: Antarctic records of precession-paced insolation-driven warming during early pleistocene marine isotope stage 31. *Geophysical Research Letters*, **35** (3), doi:10.1029/2007GL032254, URL <http://dx.doi.org/10.1029/2007GL032254>.

547 Schmitt, R., P. Bogden, and C. Dorman, 1989: Evaporation minus precipitation and density flux for the North Atlantic. *J. Phys. Oceanogr.*, (19), 1208–1221.

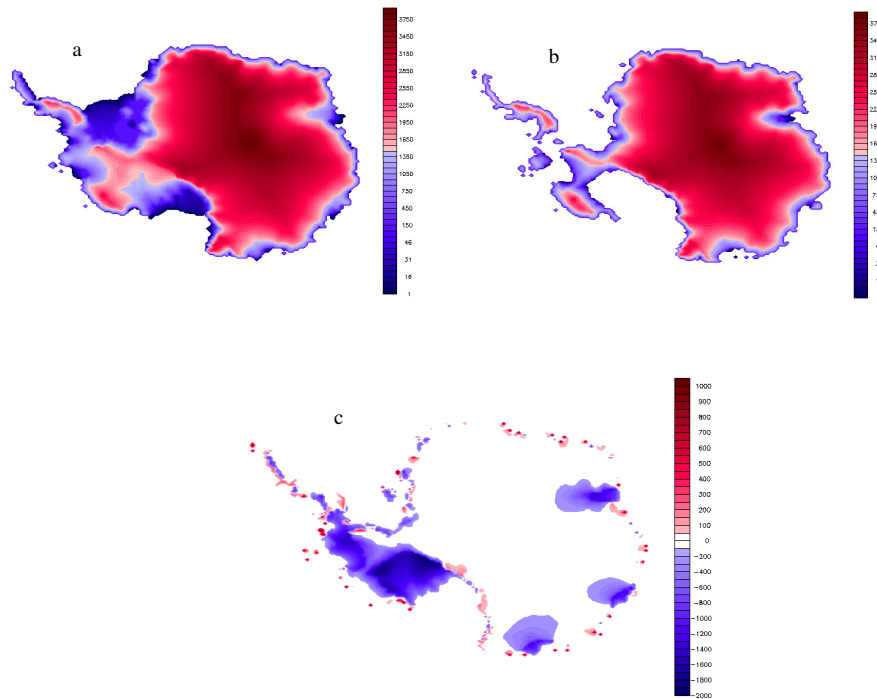
548

- 549 Severijns, C. A., and W. Hazeleger, 2010: The efficient global primitive equation climate model  
550 SPEEDO V2.0. *Geosci. Model Dev.*, **3**, 105–122, doi:10.5194/gmd-3-105-2010.
- 551 Speer, K., S. R. Rintoul, and B. Sloyan, 2000: The diabatic deacon cell. *J. Phys. Oceanogr.*, **30**.
- 552 Speer, K., and E. Tziperman, 1992: Rates of water mass formation in the North Atlantic Ocean. *J.*  
553 *Phys. Oceanogr.*, **22**, 94–104.
- 554 Stouffer, R., D. Seidov, and B. Haupt, 2007: Climate Response to External Sources of Freshwater:  
555 North Atlantic versus the Southern Ocean. *J. Climate*, **20**, 436–448.
- 556 Streng, M., O. Esper, and J. Wollenburg, 2011: Calcareous dinoflagellate cysts from  
557 the pleistocene (marine isotope stage 31) of the ross sea, antarctica. *Antarctic Science*,  
558 **23**, 597–604, doi:10.1017/S0954102011000605, URL [http://journals.cambridge.org/article\\_](http://journals.cambridge.org/article_S0954102011000605)  
559 [S0954102011000605](http://journals.cambridge.org/article_S0954102011000605).
- 560 Swingedouw, D., T. Fichefet, P. Huybrechts, H. Goosse, E. Driesschaert, and M.-F. Loutre, 2008:  
561 Antarctic ice-sheet melting provides negative feedbacks on future climate warming. *Geophysi-*  
562 *cal Research Letters*, **35** (17), n/a–n/a, doi:10.1029/2008GL034410, URL [http://dx.doi.org/10.](http://dx.doi.org/10.1029/2008GL034410)  
563 [1029/2008GL034410](http://dx.doi.org/10.1029/2008GL034410).
- 564 Whitehouse, P. L., M. J. Bentley, and A. M. L. Brocq, 2012: A deglacial model for antarc-  
565 tica: geological constraints and glaciological modelling as a basis for a new model of  
566 antarctic glacial isostatic adjustment. *Quaternary Science Reviews*, **32** (0), 1 – 24, doi:  
567 <http://dx.doi.org/10.1016/j.quascirev.2011.11.016>, URL [http://www.sciencedirect.com/science/](http://www.sciencedirect.com/science/article/pii/S0277379111003726)  
568 [article/pii/S0277379111003726](http://www.sciencedirect.com/science/article/pii/S0277379111003726).
- 569 Zachos, J., M. Pagani, L. Sloan, E. Thomas, and K. Billups, 2001: Trends, Rhythms, and Aberra-  
570 tions in Global Climate 65 Ma to Present. *Science*, doi:10.1126/science.1059412.

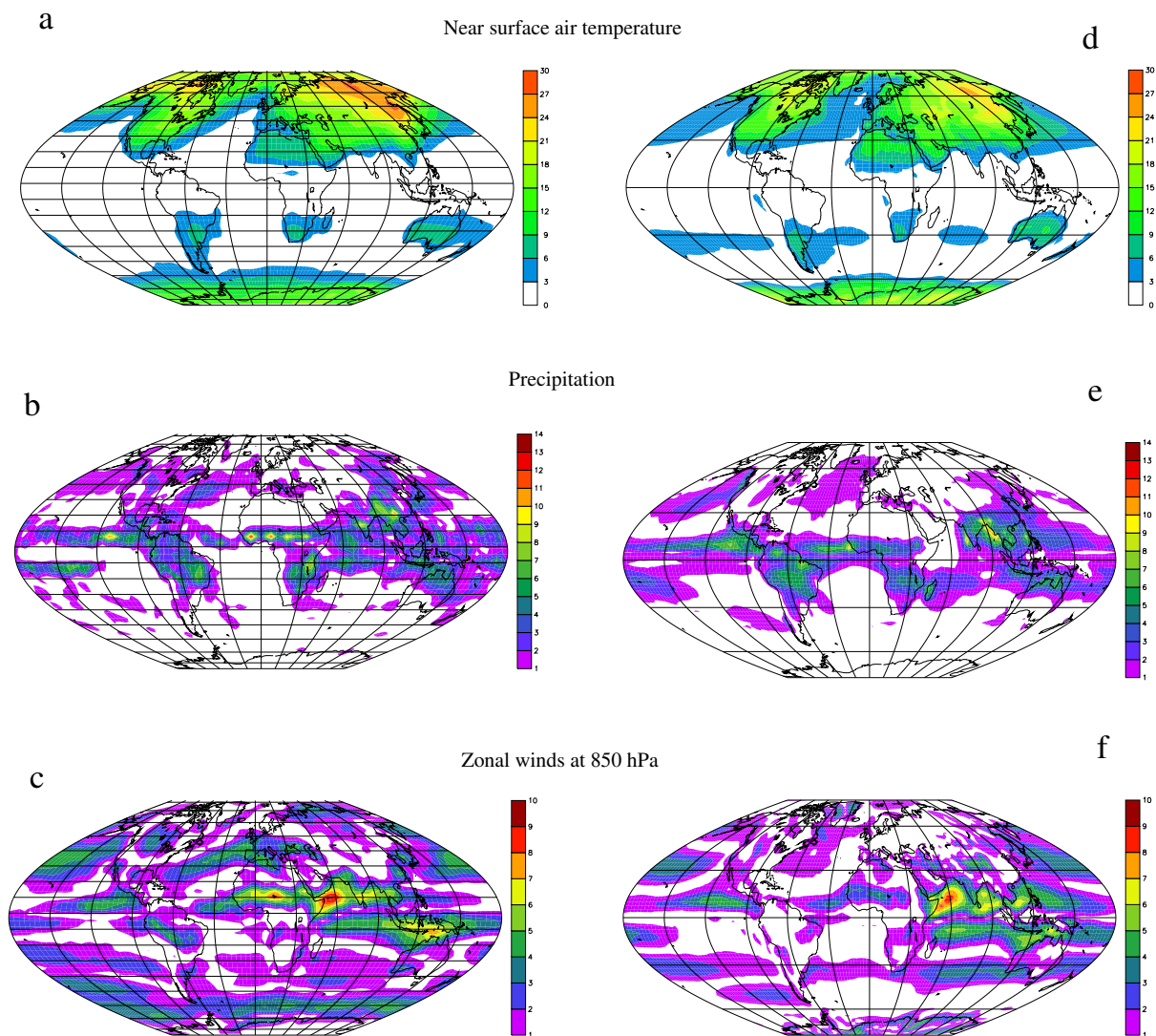
571 Zhang, Z. S., and Coauthors, 2012: Pre-industrial and mid-pliocene simulations with noresm-l.  
572 *Geoscientific Model Development*, **5** (2), 523–533, doi:10.5194/gmd-5-523-2012, URL [http:](http://www.geosci-model-dev.net/5/523/2012/)  
573 [//www.geosci-model-dev.net/5/523/2012/](http://www.geosci-model-dev.net/5/523/2012/).

## LIST OF FIGURES

575	<b>Fig. 1.</b>	Present day topography (a), WICE-EXP topography (b) and the differences between the WICE-EXP and MOD simulation (c). The unit is meter . . . . .	29
576			
577	<b>Fig. 2.</b>	(a) Amplitude of the first harmonic of the near surface air temperature [ $^{\circ}\text{C}$ ], (b,c) is the amplitude for precipitation [mm/day] and the zonal winds [m/s] at 850 hPa for MOD simulation. (d, e and f) is the same but for the NNR1 and GPCP datasets . . . . .	30
578			
579			
580	<b>Fig. 3.</b>	(a) Zonally averaged precipitation [mm/day] and (b) near surface air temperature [ $^{\circ}\text{C}$ ]. The black (red) line is for MOD simulation (GPCP and NNR1) . . . . .	31
581			
582	<b>Fig. 4.</b>	(a) Annually averaged near surface temperature ( $^{\circ}\text{C}$ ) for the MOD simulation and (b) is the differences between the WICE-EXP and MOD simulations. (c) and (d) are the same but for zonal winds, (e) and (f) are the same as in (a) and (b) but for the geopotential height at 700hPa [meters]. (g) and (h) are the same as in (e) and (f) but for precipitation (mm/day). Dotted regions are statistically significant at 95% level based on student t-test. . . . .	32
583			
584			
585			
586			
587	<b>Fig. 5.</b>	(a) Z700 [m], (b) near surface temperature [ $^{\circ}\text{C}$ ], (c) near zonal wind (m/s) response associated with the positive phase of Southern Annular Mode in the MOD simulation. (d), (e) and (f) show differences between the WICE-EXP and MOD simulations. The patterns are displayed as amplitudes by regressing hemispheric climate anomalies upon the standardized first principal component time series. Please note that figures are shown with different labels. . . . .	33
588			
589			
590			
591			
592	<b>Fig. 6.</b>	Annually averaged sea surface temperature (SST, $^{\circ}\text{C}$ ) for the MOD simulation and (b) the differences between the WICE-EXP and MOD simulations. (c) Annually averaged seaice thickness for MOD, and (d) is the differences between the WICE-EXP and MOD simulations. Dotted regions are statistically significant at 95% level based on student t-test. (e) is the all-basin annually zonally averaged vertical ocean temperatures differences between the WICE-EXP and the MOD simulation. (f) is the same as (e) but averaged only in the Atlantic basin. . . . .	34
593			
594			
595			
596			
597			
598			
599	<b>Fig. 7.</b>	(a) Meridional overturning circulation for the MOD simulation, global ocean (shaded) and the Atlantic (contour). b) is the differences between the WICE-EXP and MOD simulations (a). Annually averaged annual density flux in MOD [ $10^{-6} \times \text{kgm}^{-2}\text{s}^{-1}$ ]. (c) thermal contribution, (d) haline contribution and (e) thermal+haline. (f), (g) and (h) the same as a,b,c but for the differences between the WICE-EXP and the MOD simulation. . . . .	35
600			
601			
602			
603			



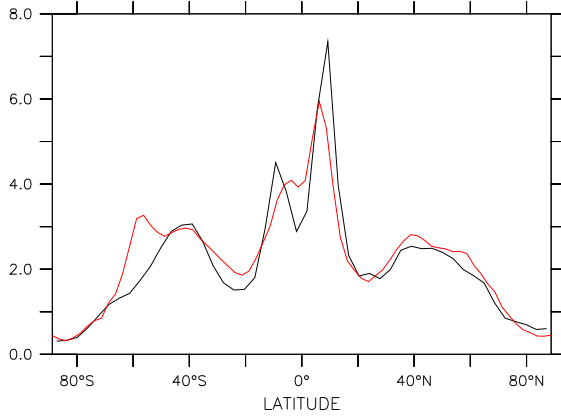
604 FIG. 1. Present day topography (a), WICE-EXP topography (b) and the differences between the WICE-EXP  
 605 and MOD simulation (c). The unit is meter



604 FIG. 2. (a) Amplitude of the first harmonic of the near surface air temperature [ $^{\circ}\text{C}$ ], (b,c) is the amplitude for  
 605 precipitation [mm/day] and the zonal winds [m/s] at 850 hPa for MOD simulation. (d, e and f) is the same but  
 606 for the NNR1 and GPCP datasets

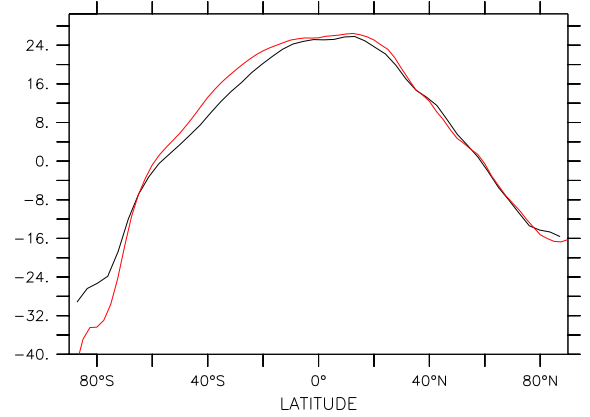


LONGITUDE : 0E to 0E(360) (XT ave)



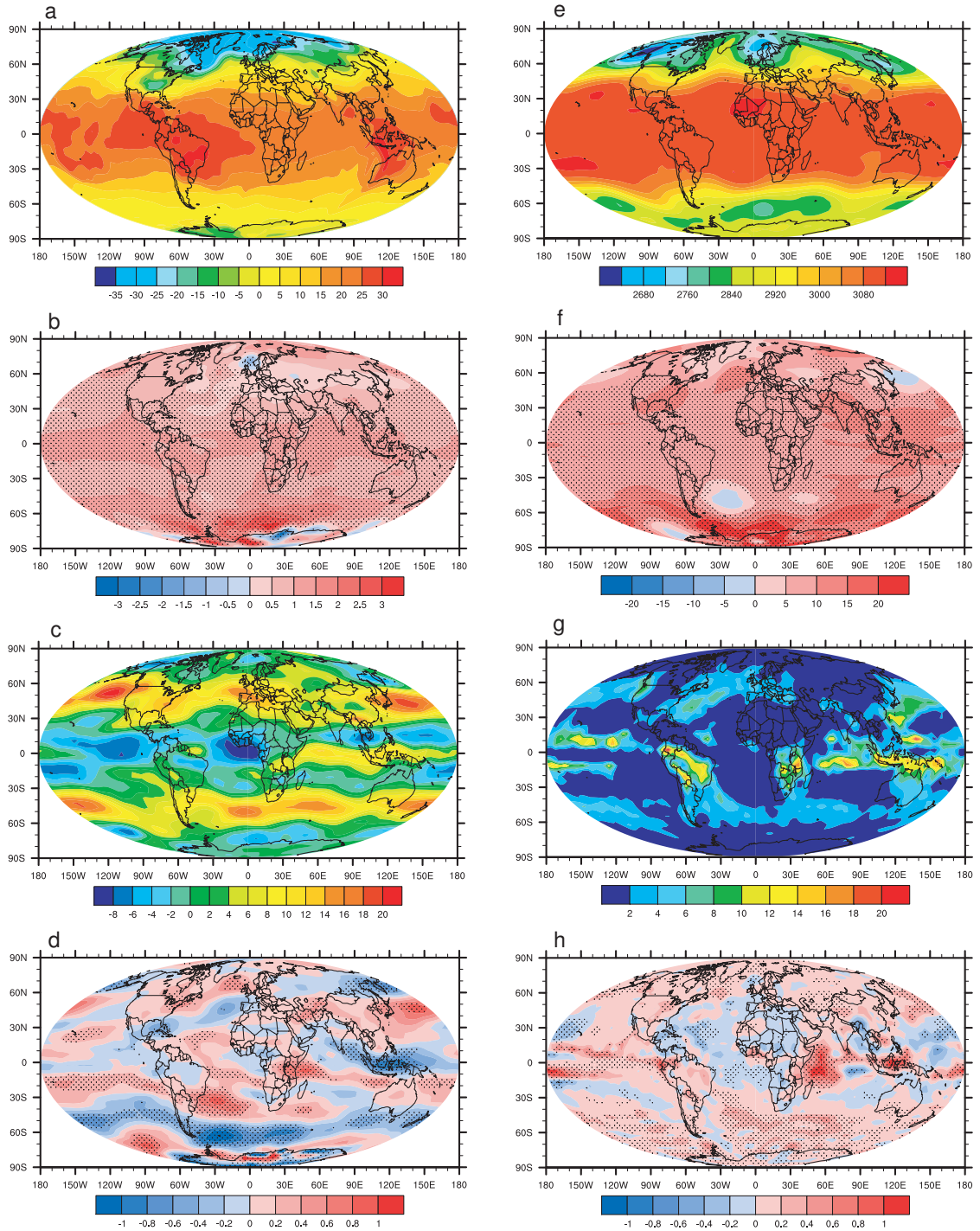
a) Precipitation – Zonal Mean (mm/day)

LONGITUDE : 0E to 0E(360) (XT ave)

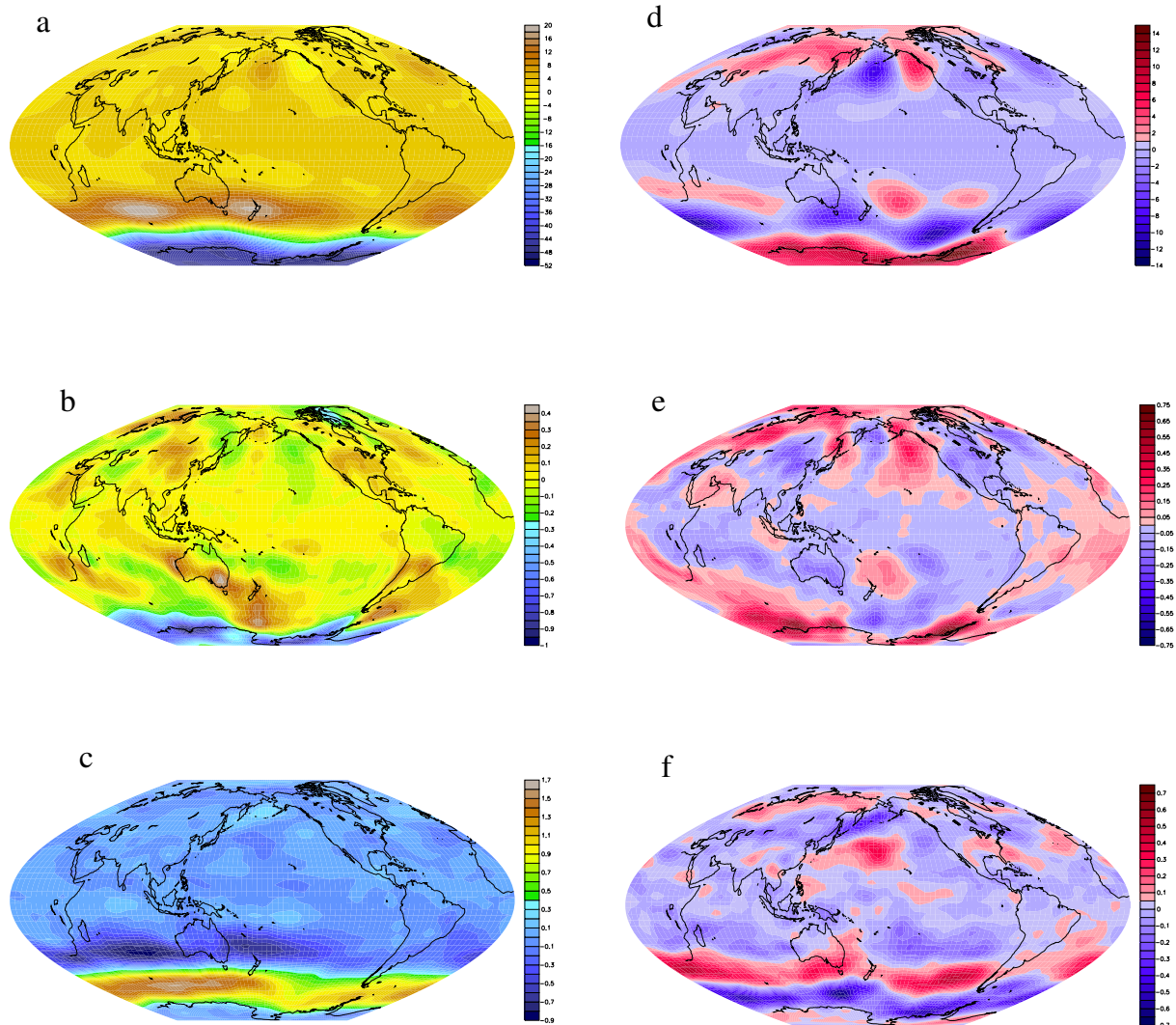


b) Near Surface Temperature – Zonal Mean (C)

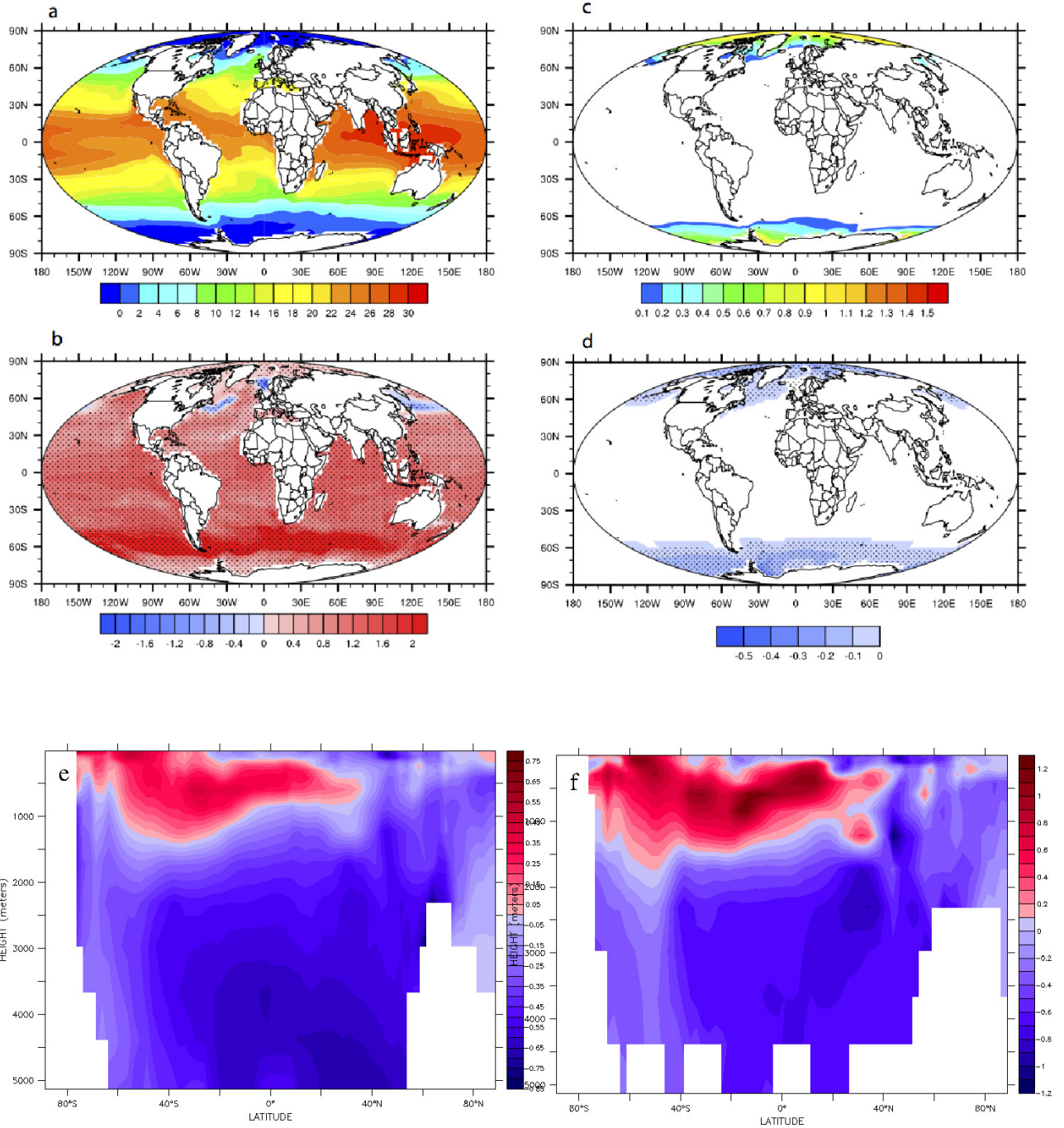
604 FIG. 3. (a) Zonally averaged precipitation [mm/day] and (b) near surface air temperature [°C]. The black (red)  
605 line is for MOD simulation (GPCP and NNR1)



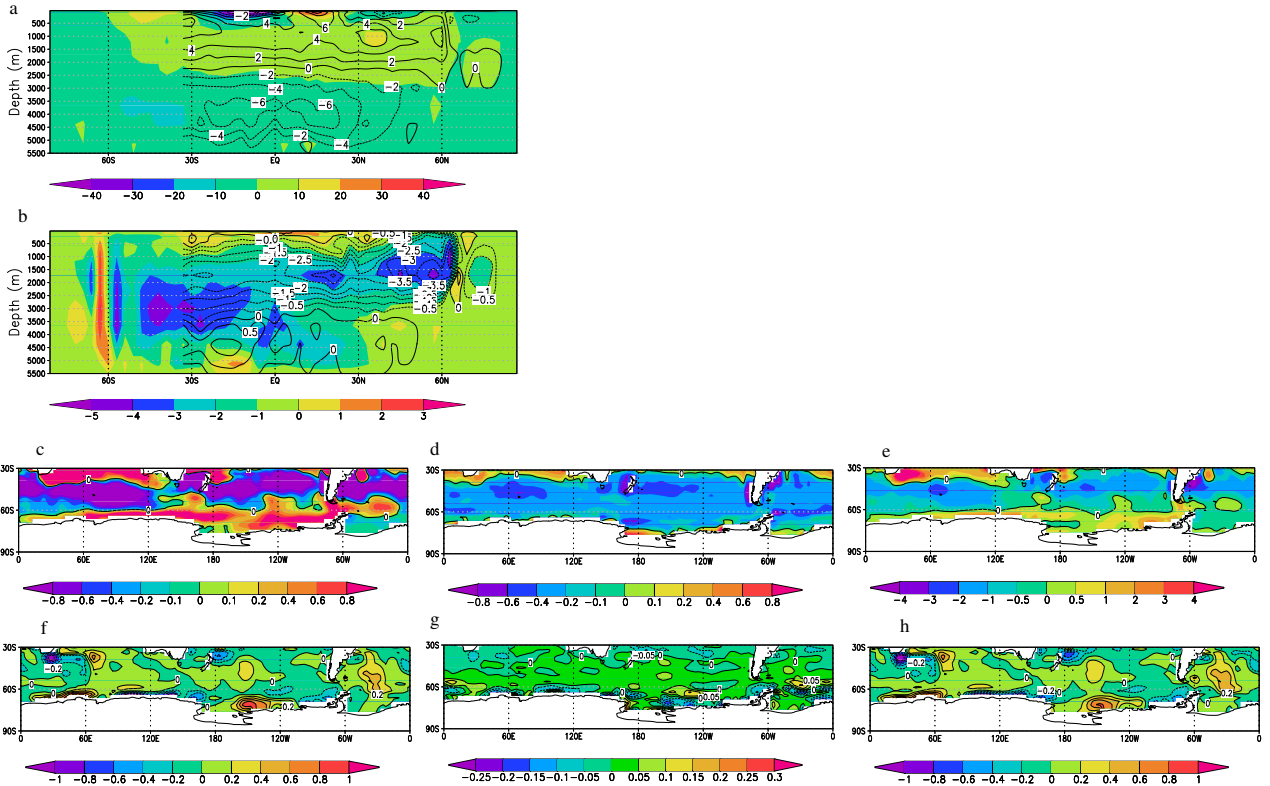
604 FIG. 4. (a) Annually averaged near surface temperature ( $^{\circ}\text{C}$ ) for the MOD simulation and (b) is the differences  
 605 between the WICE-EXP and MOD simulations. (c) and (d) are the same but for zonal winds, (e) and (f) are the  
 606 same as in (a) and (b) but for the geopotential height at 700hPa [meters]. (g) and (h) are the same as in (e) and (f)  
 607 but for precipitation (mm/day). Dotted regions are statistically significant at 95% level based on student t-test.



604 FIG. 5. (a) Z700 [m], (b) near surface temperature [ $^{\circ}$ C], (c) near zonal wind (m/s) response associated with the  
 605 positive phase of Southern Annular Mode in the MOD simulation. (d), (e) and (f) show differences between the  
 606 WICE-EXP and MOD simulations. The patterns are displayed as amplitudes by regressing hemispheric climate  
 607 anomalies upon the standardized first principal component time series. Please note that figures are shown with  
 608 different labels.



604 FIG. 6. Annually averaged sea surface temperature (SST, °C) for the MOD simulation and (b) the differences  
 605 between the WICE-EXP and MOD simulations. (c) Annually averaged sea ice thickness for MOD, and (d) is  
 606 the differences between the WICE-EXP and MOD simulations. Dotted regions are statistically significant at  
 607 95% level based on student t-test. (e) is the all-basin annually zonally averaged vertical ocean temperatures  
 608 differences between the WICE-EXP and the MOD simulation. (f) is the same as (e) but averaged only in the  
 609 Atlantic basin.



604 FIG. 7. (a) Meridional overturning circulation for the MOD simulation, global ocean (shaded) and the At-  
 605 lantic (contour). (b) is the differences between the WICE-EXP and MOD simulations (a). Annually averaged  
 606 annual density flux in MOD [ $10^{-6} \times kgm^{-2}s^{-1}$ ]. (c) thermal contribution, (d) haline contribution and (e) ther-  
 607 mal+haline. (f), (g) and (h) the same as a,b,c but for the differences between the WICE-EXP and the MOD  
 608 simulation.